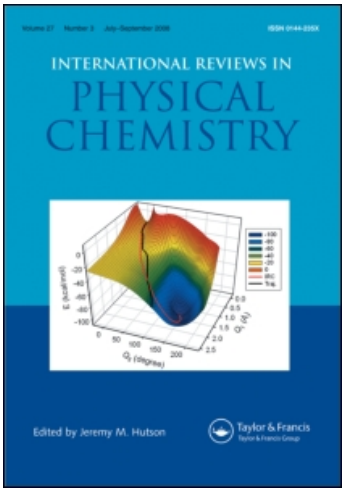

International Reviews in Physical Chemistry
Publication details, including instructions for authors and subscription information:
http://www.informaworld.com/smpp/title~content=t713724383

Singlet-to-triplet energy transfer within metal-rare gas van der Waals complexes

W. H. Breckenridge[a]
[a] Department of Chemistry, University of Utah, Salt Lake City, UT, USA

To cite this Article Breckenridge, W. H.(1994) 'Singlet-to-triplet energy transfer within metal-rare gas van der Waals complexes', International Reviews in Physical Chemistry, 13: 2, 291 — 308
To link to this Article: DOI: 10.1080/01442359409353297
URL: http://dx.doi.org/10.1080/01442359409353297

INTERNATIONAL REVIEWS IN PHYSICAL CHEMISTRY, 1994, VOL. 13, NO. 2, 291–308

Singlet-to-triplet energy transfer within metal–rare gas van der Waals complexes

by W. H. BRECKENRIDGE
Department of Chemistry, University of Utah,
Salt Lake City, UT 84112, USA

Experiments and *ab-initio* calculations are discussed involving singlet-to-triplet deactivation of group 2 and 12 metal atom *nsnp*(^{1}P) to *nsnp*(^{3}P) valence excited states induced by 'full' and 'half-collisions' with rare-gas (RG) atoms. The evidence presented is consistent with a mechanism originally postulated by Breckenridge and Malmin; if an attractive M·RG($^1\Pi_1$) potential curve is crossed by the repulsive M·RG($^3\Sigma_1^+$) potential curve below the energy region accessed experimentally, predissociation may occur to form the M(*nsnp* $^3P_2$) state. The efficiency of this singlet-to-triplet energy transfer process depends on the magnitude of the spin–orbit coupling which mixes the $^1\Pi_1$ and $^3\Sigma_1^+$ states in the curve-crossing region.

1. Introduction

It was known even in the early days before the use of lasers in chemical dynamics (Breckenridge and Umemoto 1982, Breckenridge 1983) that the conservation of spin angular momentum (Laidler 1942, 1947) 'rule' is often violated (Breckenridge and Umemoto 1982, Breckenridge 1983). In fact, in some cases, spin-forbidden processes were known to *dominate* even when there were quite exothermic spin-allowed chemical or physical exit channels readily available (Breckenridge and Malmin 1979, 1981, Breckenridge and Umemoto 1982, Breckenridge 1983). It has now been observed experimentally that species as inert as rare-gas (RG) atoms can sometimes collisionally deactivate singlet excited states of metal atoms to their lower-lying triplet states (Breckenridge and Malmin 1979, 1981, Breckenridge and Merrow 1988, Funk and Breckenridge 1989, Umemoto *et al.* 1992).

Several years ago, Breckenridge and Malmin (1981) proposed a general mechanism for such singlet-to-triplet collisional deactivation which has stood the test of time remarkably well. The mechanism is illustrated for the deactivation of Cd(5s5p $^1P_1$) to Cd(5s5p $^3P_2$) by RG atoms. Shown in figure 1 are the potential curves which result from the van der Waals interactions of the Ar atom with the first excited (5s5p $^1P_1$) singlet state and first excited (5s5p $^3P_{2,1,0}$) triplet states of the Cd atom (Kowalski *et al.* 1985, Kvaran *et al.* 1988, Funk *et al.* 1989, Wallace 1991, Bennett and Breckenridge 1992). The curves have either been constructed to fit data from laser-induced fluorescence (LIF) experiments on the cold Cd·Ar van der Waals molecule (Kowalski *et al.* 1985, Kvaran *et al.* 1988, Funk *et al.* 1989, Wallace 1991, Bennett and Breckenridge 1992) in a supersonic jet, or estimated from an empirical treatment of spin–orbit coupling (Bennett and Breckenridge 1992). These potential curves can be understood qualitatively in the following way. σ alignment of the Cd(5p) orbital is more attractive at very long range, since the axial 5pσ electron density provides a greater dispersive attraction along the bond axis. However, Cd(5pσ)·Ar(3pσ) electron–electron repulsion also sets in at very large distances. Hence, the Cd(5s5p $^1P_1$)·Ar($^1\Sigma^+$) state is *essentially* repulsive but has a very shallow potential minimum at large R. In contrast, for π alignment of the

0144-235X/94 $10·00

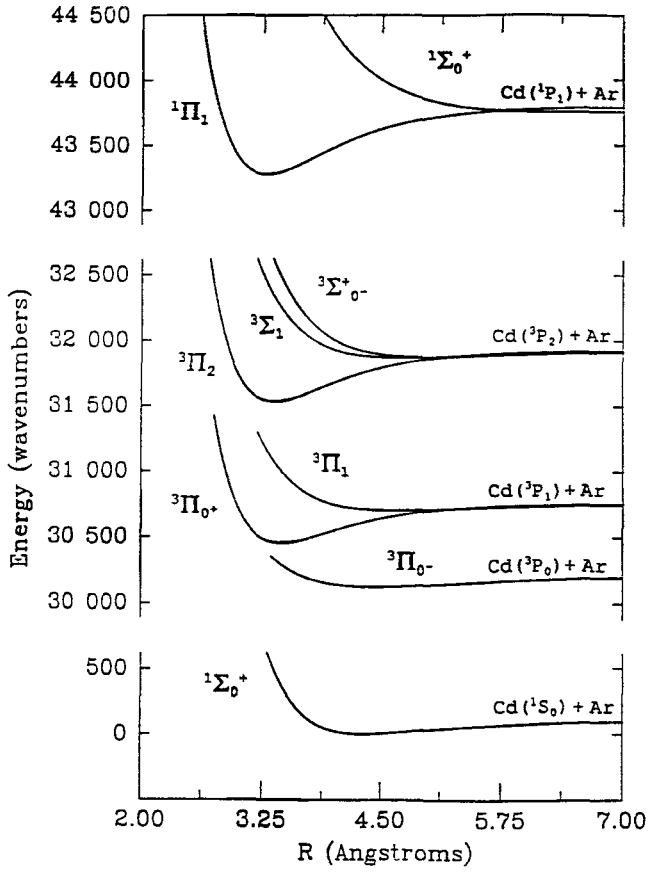

Figure 1. Morse-function estimates of the potential curves of ground state and the first excited triplet and singlet states of the Cd·Ar van der Waals molecule correlating with Ar($3p^6\ ^1S_0$) and Cd($5s5s\ ^1S_0$), Cd($5s5p\ ^3P_J$) and Cd($5s5p\ ^1P_1$) respectively (Kowalski *et al.* 1985, Kvaran *et al.* 1988, Funk *et al.* 1989, Wallace 1991, Bennett and Breckenridge 1992). Details about the construction of the potentials may be found in the work by Wallace (1991).

Cd(5p) orbital, the dispersive attraction is *less* at large R but, because the Ar atom is approaching along the nodal axis of the $5p\pi$ orbital, electron–electron repulsion does not become appreciable until much smaller values of R. The argon atom can thus penetrate closer to the $Cd(5s)^+$ 'core', which is relatively unshielded by the diffuse and transversely aligned Cd($5p\pi$) orbital. The Cd($5s5p\ ^1P_1$)·Ar($^1\Pi_1$) state is therefore much more strongly bound and has a rather small R_e (Figure 1).

Similar considerations apply to the lower-lying *triplet* σ and π states which correlate with the Cd($5s5p\ ^3P_J$) + Ar($^1S_0$) atomic states, but the coupling between spin and orbital angular momentum for such states complicates the picture somewhat (Bennett and Breckenridge 1992). In the Cd($5s5p\ ^3P_J$) case, spin–orbit coupling is quite large, and the splitting between the Cd($5s5p\ ^3P_{0,1,2}$) asymptotic levels can be comparable with or greater than the electrostatic interactions (attraction or repulsion) with Ar at moderate distances R. Thus Hund's case 'c' is approached, where the only good quantum number is Ω (Hund's case 'a' notation is still used in figure 1 since it is

more familiar to most readers). The states with the same value of Ω (and the same overall parity) interact strongly and thus can have 'mixed' $p\pi$ and $p\sigma$ alignment character (Bennett and Breckenridge 1990, 1992, Bennett *et al.* 1990). The $^3\Pi_2$ and $^3\Pi_{0+}$ states (figure 1) remain 'pure π' in nature, but the $^3\Pi_1$ and $^3\Pi_{0-}$ states are mixed (by the l^-s^+ component of the spin–orbit operator) with the $^3\Sigma_1^+$ and $^3\Sigma_{0^-}^+$ states respectively (Lefebvre-Brion and Field 1986). Because of the $p\sigma$ character which is thereby introduced into their wavefunctions by the spin–orbit interaction, the latter two $^3\Pi$ states are only quite weakly bound.

At smaller internuclear distances, and much higher energies (comparable with the $^1\Pi_1$ state energies near 43 500 cm^{-1}; figure 2), where all the triplet states are repulsive, a Hund's case 'a' description *will* be appropriate, since the electrostatic interactions are much greater than the spin–orbit coupling constant. The $^3\Sigma^+$ states are more repulsive than the $^3\Pi$ states at small R, and the $^3\Sigma_1^+$ curve could cross the bound $^1\Pi_1$ potential curve. If so, these two states (which both have $\Omega = 1$) would also be strongly mixed near the crossing region (again, by the l^+s^- component of the spin–orbit operator (Lefebvre-Brion and Field 1986)). Thus a collision in which the Cd(5s5p $^1P_1$) state is 'π aligned' with an Ar atom would begin on the bound $^1\Pi_1$ potential curve but may end up on the repulsive $^3\Sigma_1^+$ curve, producing the Cd(5s5p $^3P_2$) state.

In the particular case of Cd(5s5p $^1P_1$) + Ar, the $^1\Pi_1$ and $^3\Sigma_1^+$ curves apparently do not come close in energy until high on the repulsive inner wall of the $^1\Pi_1$ curve, since the cross-section for quenching of Cd(5s5p $^1P_1$) by Ar is found to be very low, less than 0·01 $Å^2$ (Breckenridge and Malmin 1981). In contrast, the cross-section for the quenching of the Cd(5s5p $^1P_1$) state by Xe atoms is quite high, $25 \pm 5 Å^2$ (Funk and Breckenridge 1989). Also, the Cd(5s5p $^3P_2$) multiplet is the *exclusive* product of the deactivation process by Xe atoms; *no* Cd(5s5p $^3P_1$) or Cd(5s5p $^3P_0$) was detected, entirely consistent with the Breckenridge–Malmin mechanism.

In this paper, recent experiments are discussed in which singlet-to-triplet deactivation processes are initiated and studied in a rather unique way. Instead of exciting the M(*ns*np $^1P_1$) states and letting them undergo random 'full' collisions with a quencher Q (a RG atom or a molecule), the ground-state M·RG van der Waals complex is first prepared and cooled and the M(*ns*np $^1P_1$) state is excited *within* the complex. The M(*ns*np $^1P_1$) state then undergoes 'half' a collision which may produce the M(*ns*np $^3P_2$) product. The technique has allowed detailed dynamic and spectroscopic information about the singlet-to-triplet energy-transfer processes to be obtained, all of which supports the basic idea of the Breckenridge–Malmin mechanism.

2. Spectroscopy of M(*ns*np $^1P_1$)·RG complexes

When ground-state metal vapour M is expanded in a high pressure of RG (or RG mixtures) through a nozzle into a supersonic free jet, weakly bound ground-state M(*ns*ns $^1S_0$)·RG van der Waals molecules are synthesized and cooled to their lowest vibrational level, $v'' = 0$ (Kowalski *et al.* 1985, Kvaran *et al.* 1988, Funk and Breckenridge 1989, Funk *et al.* 1989, Bennett and Breckenridge 1990, 1992, Bennett *et al.* 1990, Wallace 1991). The distribution of rotational eigenstates of the M·RG($v'' = 0$) complexes usually corresponds to a Boltzmann 'temperature' of around 10 K. As can be seen in figure 1 for the Cd·Ar example, laser excitation of the CdAr($v'' = 0$) state ($R_e'' = 4{\cdot}3$ Å) will populate high-v' levels of the Cd(5s5p $^1P_1$)·Ar($^1\Pi_1$) state (owing to Franck–Condon overlap with outer-limb portions of the v' nuclear eigenfunctions) if the frequency of the dye laser is tuned somewhat to the *red* of the Cd(5s5p $^1S_0$) atomic

transition at 43 692 cm^{-1}. Shown in figure 2 is a low-resolution LIF spectrum (Funk *et al.* 1989) of CdAr($^1\Pi_1 \leftarrow X\ ^1\Sigma^+$) vibrational transitions from $v''=0$ to $v'=4$–11. High-resolution spectra of each band reveal blue-shaded rotational structure which can be simulated with the P,Q,R branches and line strengths of a $^1\Pi_1 \leftarrow ^1\Sigma^+$ transition (figure 3). The structure is actually due to overlapped P,Q,R transitions of the several isotopomers of CdAr, and the isotopic splittings of the P band heads allow the assignment of the v' levels in the upper state (Funk *et al.* 1989).

In contrast, when the excitation frequency is scanned to the *blue* of the Cd(5s5p $^1P_1 \leftarrow$ 5s5s $^1S_0$) transition, only continuous emission with no detectable structure is observed. This is because the upper Cd(5s5p $^1P_1$)·Ar($^1\Sigma^+$) state is even more weakly bound than the Cd·Ar ground state, so that Franck–Condon excitation of Cd·Ar($v''=0$) will only access repulsive regions of the Cd(5s5p $^1P_1$)·Ar($^1\Sigma^+$) state, and the fluorescence observed is due solely to the Cd(5s5p $^1P_1$) atomic state produced after immediate dissociation of the repulsive $^1\Sigma^+$ upper state. This was proved by tuning a second laser pulse, delayed 4 ns, onto the Cd(5s5d $^1D_2 \leftarrow$ 5s5p $^1P_1$) transition, and scanning the excitation laser to the blue of the 5s5p $^1P_1 \leftarrow$ 5s5s $^1S_0$ transition (figure 4).

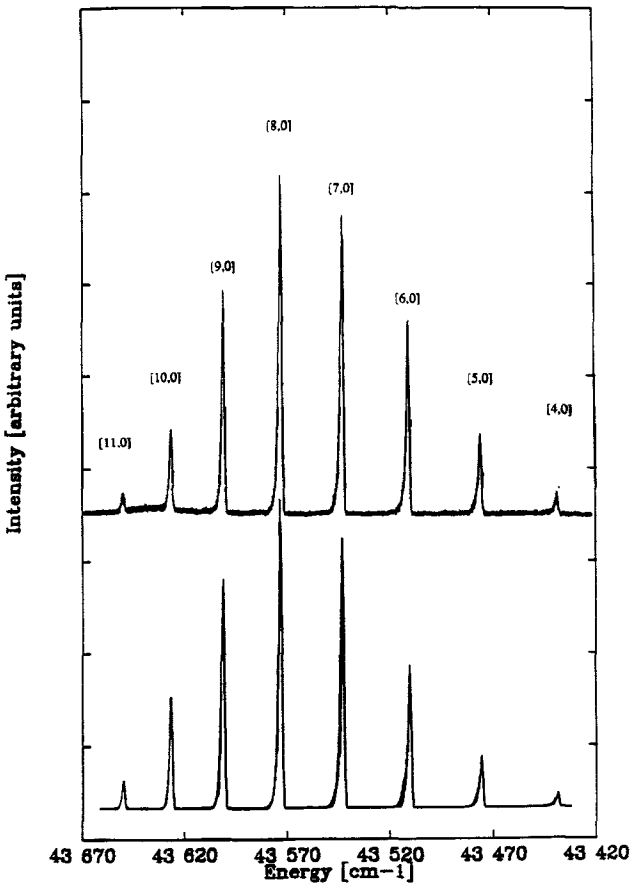

Figure 2. A low-resolution LIF spectrum showing the Cd(5s5p $^1P_1$)·Ar($^1\Pi_1, v'$) $\leftarrow$Cd(5s5s $^1S_0$)·Ar($^1\Sigma^+, v''=0$) vibrational transitions (Funk *et al.* 1989): upper curve, experimental data; lower curve, simulation. The Cd(5s5p $^1P_1 \leftarrow$ 5s5s $^1S_0$) atomic transition is at a higher energy, 43 692 cm^{-1}.

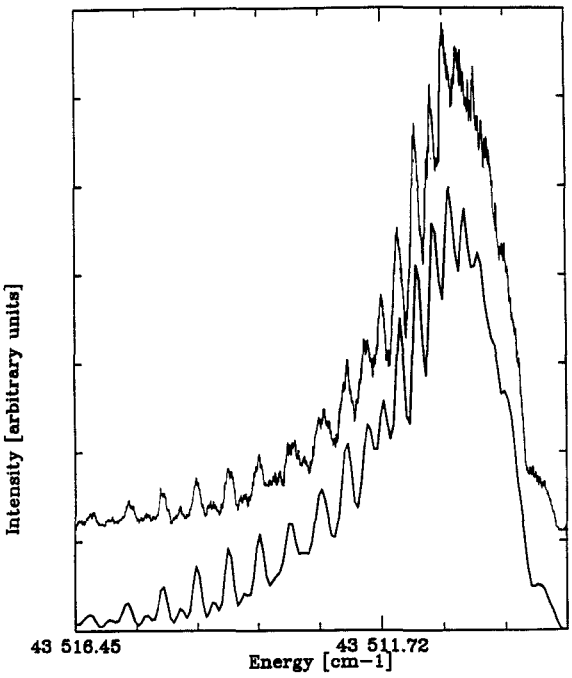

Figure 3. A higher-resolution LIF spectrum (Funk *et al.* 1989) of the (6, 0) band in figure 2, showing the overlapped P, Q, R branch rotational structure of the Cd·Ar isotopomers: upper curve, experimental data; lower curve, simulation.

The simulated spectrum is that using the $Cd(5s5p\ ^1P_1)\cdot Ar(^1\Sigma^+)$ repulsive curve and the $Cd(5s5s\ ^1S_0)\cdot Ar(^1\Sigma^+)$ ground-state curve shown in figure 1. The LIF spectroscopy of Cd·Ar is therefore completely consistent with the van der Waals bonding ideas given in the introduction. The spectroscopy of many similar M·RG species can also be rationalized by these general ideas (Breckenridge *et al.* 1994).

At this stage, some readers may wonder what this sort of spectroscopy has to do with the dynamics and mechanisms of singlet-to-triplet energy transfer. The answer, of course, is fairly obvious to those who do not insist that their science be compartmentalized and categorized, as did many spectroscopists and dynamicists when the ideas of 'half-collision' dynamics and spectroscopy were first presented several years ago! (Jouvet and Soep 1983, Breckenridge *et al.* 1986). Simply by tuning the frequency of the excitation laser, one can effect essentially complete $p\pi$ or $p\sigma$ alignment of the M(np) orbital with respect to the interaction axis and without the difficulties of crossed-beam polarized-laser type of experiments. Of course, this can also allow *direct* testing of the $^1\Pi_1$–$^3\Sigma_1^+$ Breckenridge–Malmin mechanism for singlet-to-triplet electronic energy transfer.

It is true, of course, that there is no one-to-one correspondence between 'half-collision' and 'full-collision' events. Single full collisions will *always* occur with energies *above* the M* + Q asymptotic energy, while single half-collisions can occur above *or* below the M* + Q energy (but usually below). Full collisions can occur with quite high impact parameters for efficient processes, and thus with high overall angular momentum, while half-collisions must occur with low overall angular momentum, limited by the low rotational motion of the 'cold' ground-state M·Q van der Waals

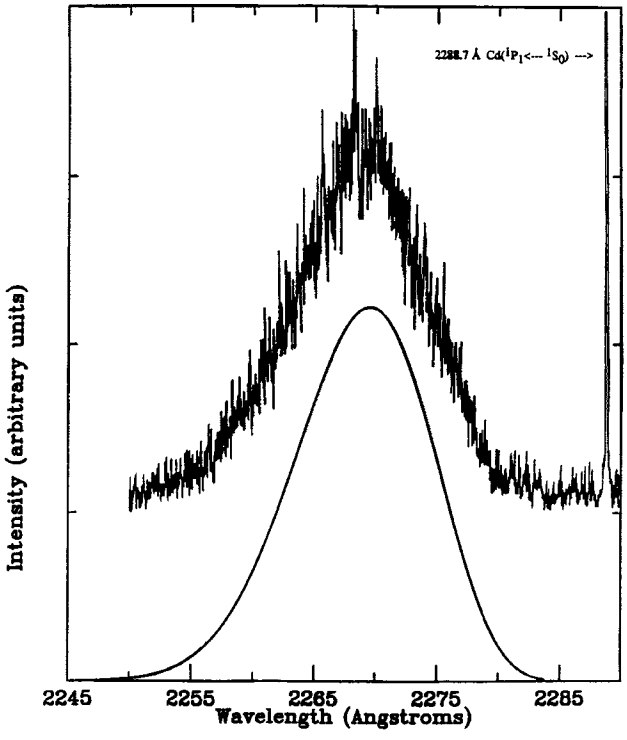

Figure 4. A Cd(5s5p $^1P_1$) 'action' spectrum of the Cd·Ar molecule to the blue of the Cd(5s5p $^1P_1 \leftarrow 5s5s\ ^1S_0$) atomic transition (Funk *et al.* 1989): upper curve, experimental data; lower curve, simulation. The excitation laser wavelength is scanned while a second laser pulse (delayed by 4 ns) is fixed onto the Cd(5s5d $^1D_2 \leftarrow 5s5p\ ^1P_1$) transition at 6440 Å. Cd($^1D_2 \rightarrow {}^1P_1$) fluorescence is collected as a function of excitation wavelength. The continuous spectrum is due to excitation of the Cd(5s5s $^1S_0$)·Ar($^1\Sigma^+, v''=0$) state to repulsive portions of the Cd(5s5p $^1P_1$)·Ar($^1\Sigma^+$) potential curve. See figure 1.

complex in the supersonic expansion. On the other hand, the M*·RG potential curves are the *same* in both cases, and the dynamic differences between full collisions and half-collisions can lead to a better understanding of singlet-to-triplet deactivation processes (Breckenridge 1989).

3. Singlet-to-triplet energy-transfer processes within M·RG complexes

3.1. *The Cd·Xe complex*

When Cd·Ne and Cd·Kr were synthesized and excited to the red of the Cd(5s5p $^1P_1 \leftarrow 5s5s\ ^1S_0$) atomic transition, LIF spectra similar to that of Cd·Ar shown in figure 2 were obtained which could be successfully simulated as $^1\Pi_1 \leftarrow {}^1\Sigma^+$ transitions (Funk *et al.* 1989). However, under conditions where Cd·Xe was *known* to be present (indicated by a strong Cd·Xe($^3\Pi_0 + \leftarrow {}^1\Sigma^+$) absorption to the red of the 5s5p $^3P_1 \leftarrow 5s5s\ ^1S_0$ atomic transition) (Kowalski *et al.* 1985, Kvaran *et al.* 1988), absolutely *no* fluorescence could be observed when the excitation laser was scanned in frequency to the red of the Cd($^1P_1 \leftarrow {}^1S_0$) transition (Funk and Breckenridge 1989).

However, when a second laser pulse was tuned to detect Cd(5s5p $^3P_2$) (by LIF), a series of broadened vibrational transitions was observed which could be assigned to

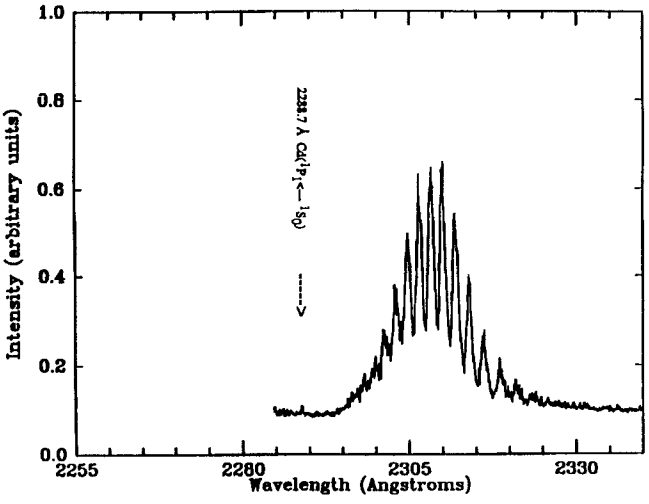

Figure 5. A Cd(5s5p $^3P_2$) 'action' spectrum of the Cd·Xe molecule to the red of the Cd(5s5p $^1P_1 \leftarrow$ 5s5s $^1S_0$) atomic transition (Funk and Breckenridge 1989). The excitation laser is scanned while a second laser pulse (delayed 4 ns) is fixed onto the Cd(5s6s $^3S_1 \leftarrow$ 5s5p $^3P_2$) atomic transition. The peaks are due to Cd(5s5p $^1P_1$)·Xe($^1\Pi_1, v'$) $\leftarrow$ Cd(5s5s $^1S_0$)·Xe($^1\Sigma^+, v''=0$) transitions severely broadened by rapid predissociation to form Cd(5s5p $^3P_2$) + Xe.

excitation of the strongly predissociated Cd(5s5p $^1P_1$)·Xe($^1\Pi_1$) state (figure 5). Consistent with the full-collision deactivation results, no Cd(5s5p $^3P_1$) or Cd(5s5p $^3P_0$) populations were detected as predissociation products. Simulations of the broadened band contours (Funk and Breckenridge 1989) were consistent with Cd·Xe($^1\Pi_1$) bound-state lifetimes of only about 0·8 ps, indicating predissociation within about one vibration. Such an efficient predissociation is, of course, consistent with the high cross-section for 'full' collisional deactivation of Cd(5s5p $^1P_1$) by Xe atoms (Funk and Breckenridge 1989). The experiments involving excitation of the Cd·Xe($^1\Pi_1$) state therefore showed *directly* that π alignment is effective for singlet-to-triplet energy transfer, entirely consistent with the Breckenridge–Malmin $^1\Pi_1$–$^3\Sigma_1^+$ crossing mechanism.

3.2. *The Zn·Xe complex*

3.2.1. *The Zn(4s4p $^1P_1$)·Xe($^1\Pi_1$) state*

The analogous $^1\Pi_1 \leftarrow X^1\Sigma^+$ transitions for Zn·Ar and Zn·Kr complexes (Wallace *et al.* 1991, 1992) have been observed by LIF to the red of the Zn(4s4p $^1P_1 \leftarrow$ 4s4s $^1S_0$) atomic transition. Shown in figures 6 and 7 are the low-resolution spectrum and a high-resolution spectrum for one band of the Zn·Kr transition (Wallace *et al.* 1992).

Similar to the Cd·Xe case, no LIF signal could be observed when an excitation laser was scanned in frequency to the red of the Zn($^1P_1 \leftarrow {}^1S_0$) transition under conditions where Zn·Xe should have been synthesized in the jet (Wallace *et al.* 1991). When a second laser pulse was fixed in frequency to detect Zn(4s4p $^3P_2$) as a pre-dissociation product, an 'action' spectrum was obtained, however, consisting of several vibrational bands with discernible isotopic and broadened rotational structure (Wallace *et al.* 1991) (figures 8 and 9). The computer simulations are consistent with Zn(5s5p $^1P_1$)·Xe($^1\Pi_1$) predissociation lifetimes on the order of 5 ps, about seven times

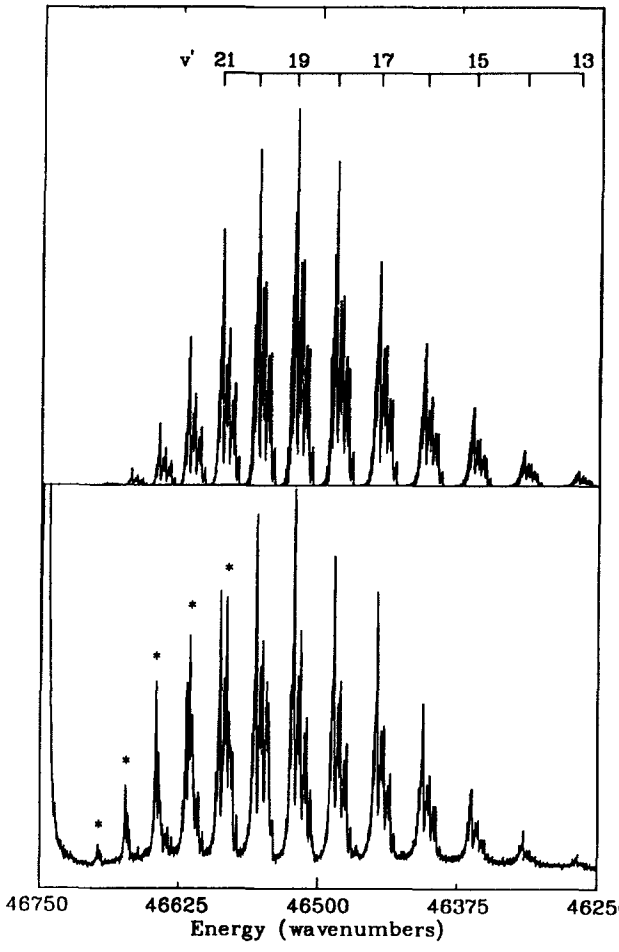

Figure 6. A low-resolution LIF spectrum showing the Zn(4s4p $^1P_1$)·Kr($^1\Pi_1, v'$)←Zn(4s4s $^1S_0$) × Kr($^1\Sigma^+, v''=0$) vibrational transitions (Wallace *et al.* 1992). The Zn(4s4p $^1P_1$←4s4s $^1S_0$) atomic transition is seen at 46 745 cm^{-1}: lower curve, experimental data; upper curve, simulation. (The asterisks indicate transitions due to small amounts of Cd·Ar present.)

longer than for the Cd(5s5p $^1P_1$)·Xe($^1\Pi_1$) state. There is thus a $^1\Pi_1$–$^3\Sigma_1$ crossing for Zn·Xe at energies below the $^1\Pi_1$ vibrational eigenstates of $v'=28$ to $v'=41$ which can be Franck–Condon *accessed* from the $v''=0$ ground state (the only Zn·Xe vibrational state observed in the ultra-cold supersonic expansion). It has been proposed (Wallace *et al.* 1991) that the longer predissociation lifetime of Zn·Xe($^1\Pi_1$) compared with Cd·Xe($^1\Pi_1$) is due to the 2·8-fold lower spin–orbit coupling for Zn(4s4p)states Cd(5s5p) states, since the predissociation rate should depend on the *square* of the spin–orbit coupling matrix element (Lefebvre-Brion and Field 1986). Given the correlation of the efficient predissociation of Cd·Xe($^1\Pi_1$) with the high cross-section for quenching of Cd(5s5p $^1P_1$) by Xe (about 25 $Å^2$), we predicted (Wallace *et al.* 1991) that the cross-section for the quenching of Zn(4s4p $^1P_1$) by Xe would likely be in the 2–5 $Å^2$ range. Umemoto *et al.* (1992) subsequently measured this cross section experimentally: 3·4 $Å^2$.

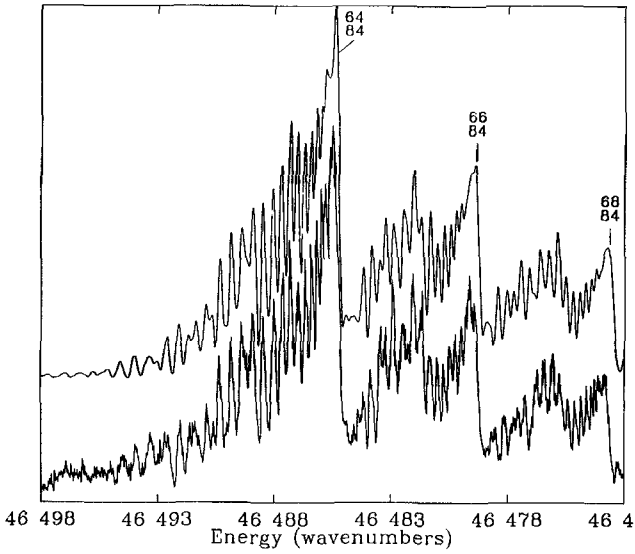

Figure 7. A higher-resolution LIF spectrum of the (18,0) band in figure 6, showing the overlapped P, Q, R branch rotational structure of the Zn·Kr isotopomers (Wallace *et al.* 1992): lower curve, experimental data; upper curve, simulation. The numbers indicate the P band-head frequencies of three major isotopomers.

In the Zn(4s4p $^1P_1$)–Xe case, a small (about 10%) yield of Zn(4s4p $^3P_1$) is also observed, in both full-collision (Umemoto *et al.* 1992) and half-collision (Wallace *et al.* 1991) studies, but no Zn(4s4p $^3P_0$) is produced. The $^3\Sigma_1^+$ state is always produced by the crossing with the $^1\Pi_1$ state on the inner limb of its potential curve (see § 3.4). Some coupling with the $^3\Pi_1$ state (both are $\Omega = 1$ states) can *then* occur, however, owing to the high Zn–Xe relative radial velocities reached on the repulsive $^3\Sigma_1^+$ curve at larger R, where the $^3\Pi_1$ and $^3\Sigma_1^+$ states are closest in energy (Wallace *et al.* 1991). The $^3\Pi_1$ component correlates asymptotically with Zn(4s4p $^3P_1$) + Xe. No Zn(4s4p $^3P_0$) can be formed by such a mechanism, since this atomic state correlates with the $^3\Pi_0$– component, which has a value of Ω different from that of the $^3\Sigma_1^+$ state. No Cd(5s5p $^3P_1$) is produced in the Cd·Xe case (Funk and Breckenridge 1989) because the Cd·Xe($^3\Sigma_1^+$) state and the Cd·Xe($^3\Pi_1$) state are about three times farther apart in energy (asymptotically) owing to the larger spin–orbit coupling in the Cd(5s5p) states; radial electronic coupling depends extremely sensitively on the energy gap ΔE between the two states (Wallace *et al.* 1991).

3.2.2. *The Zn(4s4p $^1P_1$)·Xe($^1\Sigma_0^+$) state*

When Zn·Xe is present and the excitation laser is tuned to the blue of the Zn($^1P_1 \leftarrow {}^1S_0$) atomic transition, a weak LIF spectrum was observed (Wallace *et al.* 1991) (figure 10) which could be assigned to the bound–bound portion of the Zn(4s4p $^1P_1$)·Xe($^1\Sigma_0^+$)←Zn(4s4s $^1S_0$)·Xe($^1\Sigma_0^+$) transition. Franck–Condon overlap, although extremely small even for the most intense bound–bound transition, is maximal on the inner-limb portion of the shallow Zn(4s4p $^1P_1$)·Xe($^1\Sigma^+$) potential well. The sharp sudden drop in LIF intensity occurs just at the Zn(4s4p $^1P_1$)·Xe($^1\Sigma^+$) dissociation energy. The Zn(4s4p $^1P_1$) atomic state is produced when the excitation energy is above the dissociation limit, but its resonant fluorescence is highly

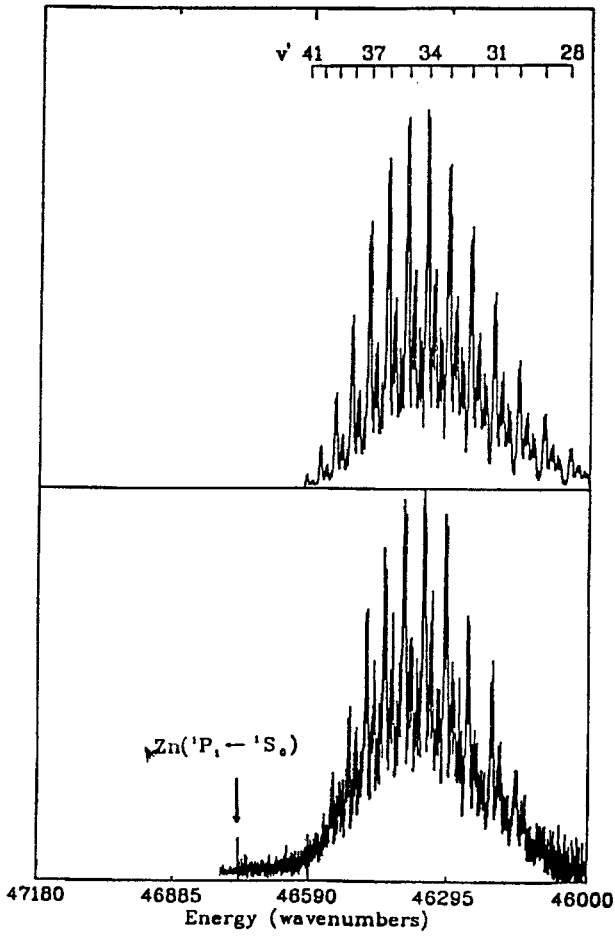

Figure 8. A Zn(4s4p $^3P_2$) 'action' spectrum of the Zn·Xe molecule to the red of the Zn(4s4p $^1P_1 \leftarrow$ 4s4s $^1S_0$) atomic transition (Wallace *et al.* 1991): lower curve, experimental data; upper curve, simulation. The excitation laser is scanned while a second laser pulse (delayed 12 ns) is fixed onto the Zn(4s5s $^3S_1 \leftarrow$ 4s4p $^3P_2$) atomic transition. The peaks are due to Zn(4s4p $^1P_1$)·Xe($^1\Pi_1, v'$)$\leftarrow$Zn(4s4s $^1S_0$)·Xe($^1\Sigma^+, v''=0$) isotopomer vibrational transitions somewhat broadened by predissociation to form Zn(4s4p $^3P_2$)+Xe.

'imprisoned' by the huge excess of ground-state Zn atoms present and diffuses out of view of the collection optics, resulting in the sharp drop in LIF intensity at the dissociation limit (Wallace *et al.* 1991).

The important point of this result with regard to singlet-to-triplet deactivation is that the Zn(4s4p $^1P_1$)·Xe($^1\Sigma_0^+$) state does *not* pre-dissociate to form Zn(^3P_J) states but lives for many, many vibrations (several nanoseconds) before *fluorescing*. This shows directly and dramatically that π alignment of the Zn(4p $^1P_1$) orbital is moderately effective for singlet-to-triplet deactivation in this case, but that σ alignment most certainly is *not*, completely consistent with the Breckenridge–Malmin mechanism.

Shown in figure 11 are the potential curves of the ZnXe molecule derived from the spectroscopic measurements, which show the huge energy differences between σ and π alignment of the Zn(4p $^1P_1$) orbital with respect to the bond axis.

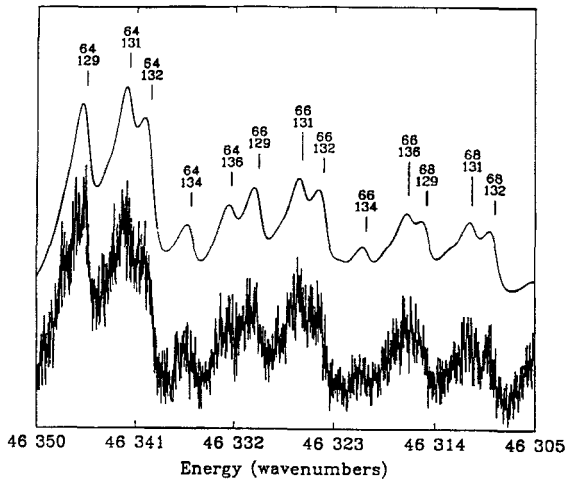

Figure 9. Higher resolution Zn($^3P_2$) 'action' spectrum (Wallace *et al.* 1991) of the (34, 0) band in figure 8: lower curve, experimental data; upper curve, simulation. The numbers indicate the P band-head frequencies of the Zn·Xe isotopomers.

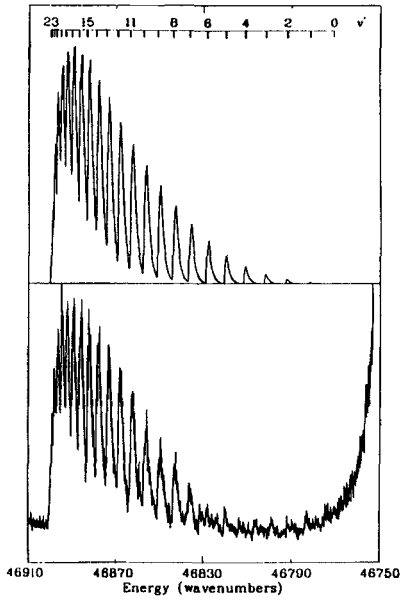

Figure 10. Low-resolution LIF spectrum showing the Zn(4s4p $^1P_1$)·Xe($^1\Sigma^+, v'$) $\leftarrow$Zn(4s4s $^1S_0$)·Xe($^1\Sigma^+, v''=0$) vibrational transitions (Wallace *et al.* 1991): lower curve, experimental data; upper curve, simulation. The Zn(4s4p $^1P_1 \leftarrow$ 4s4s $^1S_0$) atomic transition is at lower energies, 46 745 cm^{-1}.

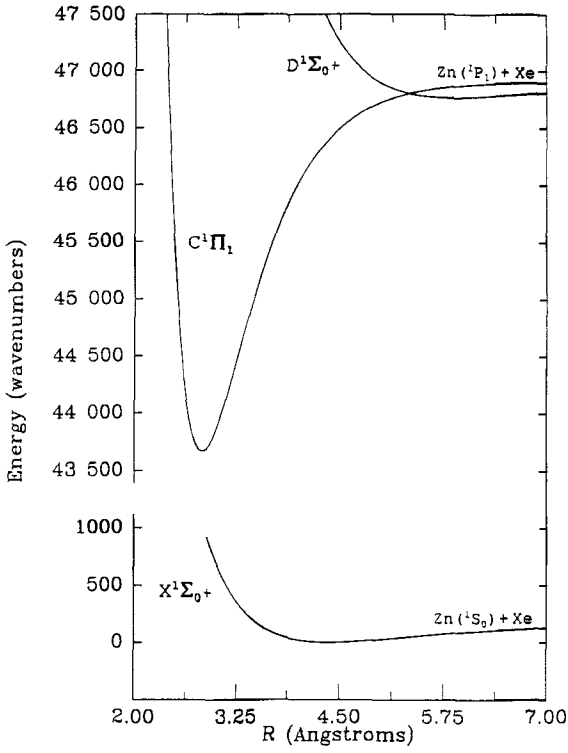

Figure 11. Potential curves of the ground state and first two singlet excited states of the Zn·Xe molecule, determined from spectroscopic measurements (Wallace *et al.* 1991).

3.3. *The Mg·Xe complex*

Since there are obvious $^1\Pi_1 - {}^3\Sigma_1^+$ potential curve crossings in the Cd·Xe and Zn·Xe cases, one might also suspect that such a curve crossing exists for the analogous Mg(3s3p $^1P_1$)·Xe($^1\Pi_1$) and Mg(3s3p $^3P_2$)·Xe($^3\Sigma_1^+$) states. However, the Mg(3s3p $^1P_1$)·Xe($^1\Pi_1$) state has been found to fluoresce strongly (McCaffrey *et al.* 1993, 1994), and very careful attempts to detect even small amounts of Mg(3s3p $^3P_2$) pre-dissociation product were unsuccessful (McCaffrey *et al.* 1993). On the other hand, it is not completely certain whether the very slow pre-dissociation rate is due to the lack of a $^1\Pi_1$–$^3\Sigma_1^+$ curve crossing or to the much lower spin–orbit coupling for the light Mg atom 3s3p states. Assuming that the pre-dissociation rate is roughly proportional to the square of the atomic spin–orbit coupling constant for the *nsnp* ^3P_J states (Lefebvre-Brian and Field 1986), one would predict from the observed Zn·Xe pre-dissociation lifetime a pre-dissociation lifetime for Mg·Xe($^1\Pi_1$) of about 500 ps, which is *shorter* than, but of the same order of magnitude as, the Mg·Xe($^1\Pi_1$) fluorescence lifetime of about 2000 ps (presumed to be the same as the free Mg(3s3p $^1P_1$) atomic state; Breckenridge and Umemoto 1982).

3.4. Ab-initio *calculations of the repulsive potential curves of M(nsnp ^3P)·RG($^3\Sigma^+$) states*

For all the M·RG cases, it is often possible to extract reasonably accurate experimental information about the bound $^1\Pi_1$ potential curves from LIF or action spectroscopy, but such information about the repulsive $^3\Sigma_1^+$ states, especially at several thousand wavenumbers above their atomic asymptotic energies where there may be a

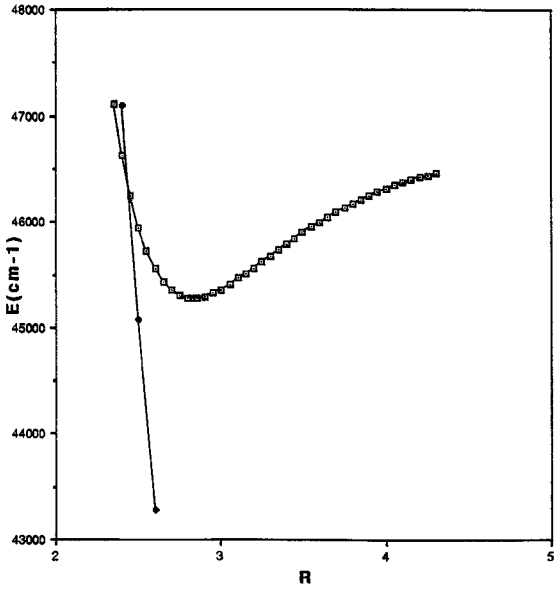

Figure 12. $Zn(4s4p\,^1P_1)\cdot Kr(^1\Pi_1)$ potential curve estimated from experimental spectroscopic measurements (Wallace *et al.* 1992) ⊡ and $Zn(4s4p\,^3P_2)\cdot Kr(^3\Sigma^+)$ potential curve estimated from the highest-level *ab-initio* calculations attempted by Bililign *et al.* (1993) (◆). It is likely that the *true* $^3\Sigma^+$ curve is slightly less repulsive than the *ab-initio* estimate (see text).

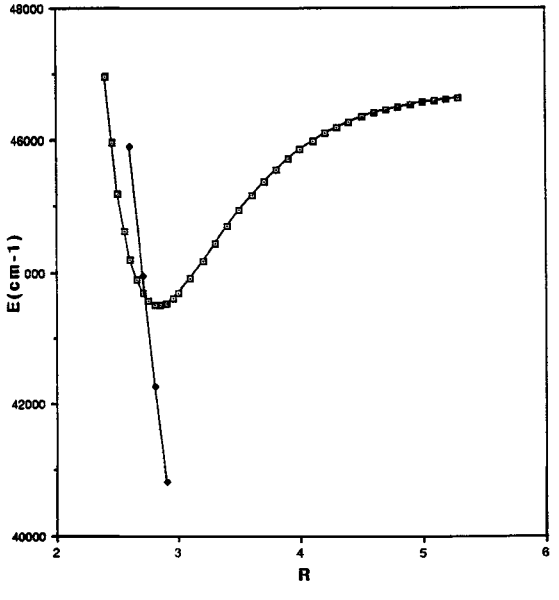

Figure 13. $Zn(4s4p\,^1P_1)\cdot Xe(^1\Pi_1)$ potential curve estimated from experimental spectroscopic measurements (Wallace *et al.* 1991) (⊡) and $Zn(4s4p\,^3P_2)\cdot Xe(^3\Sigma^+)$ potential curve estimated from the highest-level *ab-initio* calculations attempted by Bililign *et al.* (1993) (◆). It is likely that the *true* $^3\Sigma^+$ curve is slightly less repulsive than the *ab-initio* estimate (see text).

$^1\Pi_1$–$^3\Sigma_1^+$ crossing, is virtually impossible to obtain experimentally. Therefore *ab-initio* calculations of these M·RG($^3\Sigma^+$) repulsive curves were performed (Bililign *et al.* 1993) for several cases in which the bound $^1\Pi_1$ potential curves have been characterized experimentally, with the goal of examining the general $^1\Pi_1$–$^3\Sigma_1^+$ curve-crossing mechanistic ideas as well as providing more information about the true cause of the inefficient Mg(3s3p $^1P_1$)·Xe($^1\Pi_1$) predissociation.

3.4.1. *Zn·Kr*

It was found necessary in all cases to utilize very-high-quality basis sets and high levels of correlated calculations to obtain agreement with experimental observations (Bililign *et al.* 1993). There was always a regular decrease in the repulsive character of the M·RG($^3\Sigma^+$) states as the basis set quality and level of correlation was increased. (Bililign *et al.* 1993). For example, it is known that the Zn(4s4p $^1P_1$)·Kr($^1\Pi_1$) state fluoresces strongly and does not predissociate to form Zn(4s4p $^3P_2$) (Wallace *et al.* 1992). This means that the repulsive Zn(4s4p $^3P_2$)·Kr($^3\Sigma_1^+$) state does *not* cross the bound Zn(4s4p $^1P_1$)·Kr($^1\Pi_1$) state on its inner limb until energies *above* those Franck–Condon accessible (up to about 300 cm^{-1} from the dissociation limit). Shown in figure 12 is the experimentally estimated potential curve for the Zn·Kr($^1\Pi_1$) state and the *ab-initio* Zn·Kr($^3\Sigma^+$) potential curve calculated with the highest basis set quality and level of correlation attempted (Bililign *et al.* 1993). Although there is still a crossing within the experimentally accessible energy region, the *true* $^3\Sigma^+$ curve is probably just slightly less repulsive and crosses the $^1\Pi_1$ state above its dissociation limit.

3.4.2. *Zn·Xe*

Shown in figure 13 is the experimentally estimated potential curve for the ZnXe($^1\Pi_1$) state and the *ab-initio* curve calculated with the highest basis set quality and level of correlation attempted (Bililign *et al.* 1993). It can be seen that there will still be a $^1\Pi_1$–$^3\Sigma_1^+$ crossing on the inner limb of the $^1\Pi_1$ curve in this case even if the true $^3\Sigma_1^+$ curve is slightly less repulsive than the best *ab-initio* curve shown in figure 13. This 'inner-limb' crossing is consistent with the experimental results, which indicated there was no large variation in predissociation linewidth with vibrational level (Lefebvre-Brion and Field 1986, Wallace *et al.* 1991). (The lower-level *ab-initio* calculations gave 'outer-limb' $^1\Pi_1$–$^3\Sigma_1^+$ crossings, inconsistent with experiment (Lefebvre-Brion and Field 1986, Wallace *et al.* 1991, Bililign *et al.* 1993).)

3.4.3. *Mg·Xe*

Similar *ab-initio* calculations of the repulsive Mg(3s3p ^3P)·Xe($^3\Sigma^+$) state potential curve are shown in figure 14, together with the experimental estimate of the bound Mg(3s3p $^1P_1$)·Xe($^1\Pi_1$) state potential curve. Although a crossing is observed high on the $^1\Pi_1$ potential inner limb, it is likely that the Mg·Xe($^3\Sigma_1^+$) curve is *less* repulsive than the best *ab-initio* estimate, and the crossing is probably slightly above the Mg·Xe($^1\Pi_1$) dissociation limit. Thus lack of an energetically accessible $^1\Pi_1$–$^3\Sigma_1^+$ curve crossing is the likely reason for the inefficiency of Mg(3s3p $^1P_1$)–Xe singlet-to-triplet energy transfer, and not the low spin–orbit coupling for the Mg(3s3p) excited states.

3.4.4. *General conclusions*

The *ab-initio* calculations thus resulted in a better understanding of why only the Zn(4s4p $^1P_1$)·Xe($^1\Pi_1$) and Cd(4s4p $^1P_1$)·Xe($^1\Pi_1$) states predissociate to form triplet-state products (Bililign *et al.* 1993). For a given M(*nsnp*) state, as one proceeds through

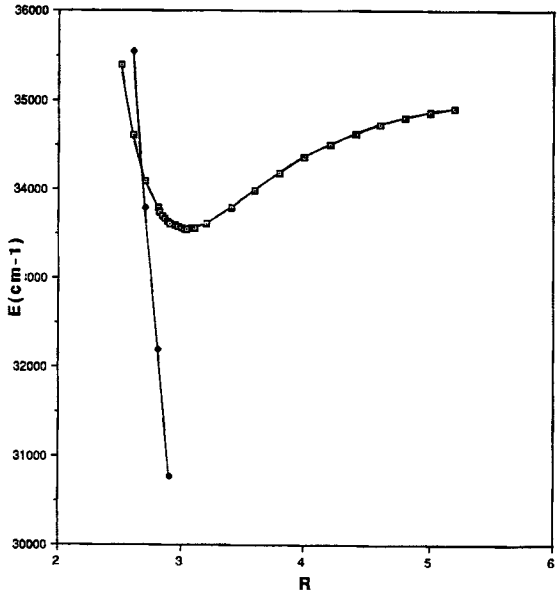

Figure 14. $Mg(3s3p\ ^1P_1)$-$Xe(^1\Pi_1)$ potential curve estimated from experimental spectroscopic measurements (McCaffrey *et al.* 1993) (⊡) and $Mg(3s3p\ ^3P_2)$-$Xe(^3\Sigma^+)$ potential curve estimated from the highest-level *ab-initio* calculations attempted by Bililign *et al.* (1993) (◆). It is likely that the *true* $^3\Sigma^+$ curve is slightly less repulsive than the *ab-initio* estimate (see text).

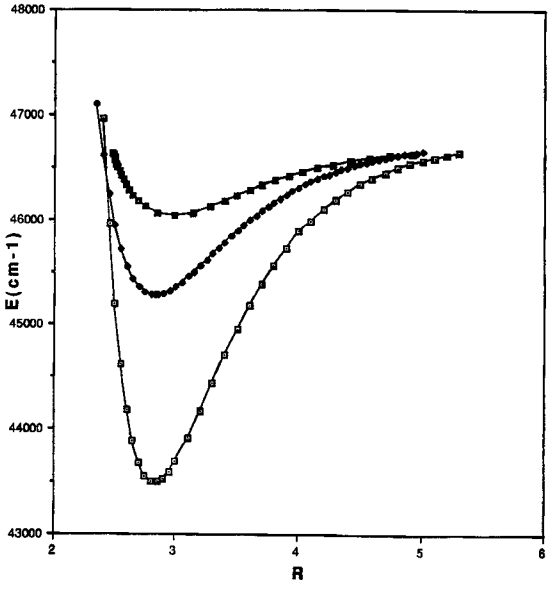

Figure 15. Excited $Zn(4s4p\ ^1P_1)$-$RG(^1\Pi_1)$ potential curves estimated from spectroscopic measurements (Wallace *et al.* 1988, 1991, 1992); (■), RG≡Ar; (◆), RG≡Kr; (⊡), RG≡Xe.

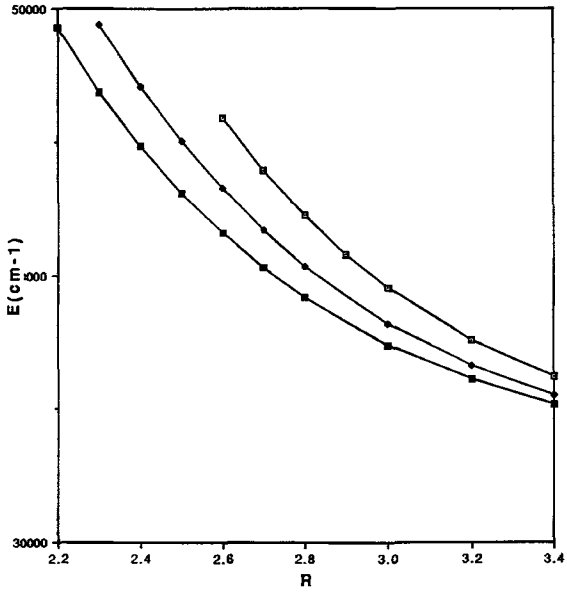

Figure 16. Excited Zn(4s4p ^{3}P)·RG($^3\Sigma^+$) potential curves estimated from high-level *ab-initio* calculations (Bililign *et al.* 1993): (■), RG ≡ Ar; (◆), RG ≡ Kr; (⊡), RG ≡ Xe.

the series RG ≡ Ne, Ar, Kr or Xe, the M(*nsnp* $^1P_1$)·RG($^1\Pi_1$) states become more attractive as the polarizability of the RG atom increases. For example, in figure 15 the Zn·Ar, Zn·Kr, Zn·Xe $^1\Pi_1$ potential curves estimated experimentally are shown (Wallace *et al.* 1988, 1991, 1992). Particularly significant is that, as D_e increases, R_e for the $^1\Pi_1$ states also actually *decreases* slightly, despite the increasing *size* of the RG atoms in the Ar, Kr, Xe series. However, for the high-energy repulsive portions of the $^3\Sigma_1^+$ curves, the increasing size of the RG atom *does* matter, resulting in *more* repulsive curves in the series Ar, Kr, Xe. This is shown clearly in figure 16, where the *ab-initio* $^3\Sigma^+$ potential curves for Zn·Ar, Zn·Kr, and Zn·Xe are shown (Bililign *et al.* 1993). It is obvious that the deeper well depths for the $^1\Pi_1$ states as well as the more repulsive nature of the $^3\Sigma_1^+$ states favour lower-energy $^1\Pi_1$–$^3\Sigma_1^+$ crossings for RG ≡ Xe.

3.5. *Is Xe a 'heavy' atom or just a 'large' atom with regard to M·RG singlet-to-triplet energy transfer?*

As discussed in the last section, the unique efficacy of RG ≡ Xe for inducing singlet-the $^1\Pi_1$ states also actually *decreases* slightly, despite the increasing *size* of the RG *bonding* trends in the $^1\Pi_1$ and $^3\Sigma_1^+$ states (more bound and more repulsive respectively), *without* invoking an increase in spin–orbit coupling because Xe serves as a 'heavy atom' (McGlynn *et al.* 1969). Here we examine further evidence that the spin–orbit coupling in the Cd(5s5p) and Zn(4s4p) (and probably even the Mg(3s3p)) states is sufficient to induce pre-dissociation of the M(*nsnp* $^1P_1$)·RG ($^1\Pi_1$) states if there is a $^1\Pi_1$–$^3\Sigma_1^+$ *curve crossing* in the energy region of the $^1\Pi_1$ potential curve below that which is *accessed experimentally*.

The spin–orbit coupling constants for the valence *nsnp* excited states of the Mg, Zn and Cd atoms are 40·6, 386 and 1142 cm^{-1}, respectively. Umemoto *et al.* (1992) have performed close-coupling calculations (following the method of Pouilly and Alexander (1987) and Alexander and Pouilly (1988)) to examine the mechanism of 'full-collision'

deactivation of Zn(4s4p $^1P_1$) to Zn(4s4p $^3P_2$) and Zn(4s4p $^3P_1$) by Xe atoms. Their results confirm strikingly the Breckenridge–Malmin mechanism (1981) and the suggestion of Wallace *et al.* (1991) that Zn(4s4p $^3P_1$) is produced by Zn·Xe $^3\Sigma_1^+$–$^3\Pi_1$ exit-channel radial coupling. They found that $^1\Pi_1$–$^3\Sigma_1^+$ coupling peaked strongly and locally near the $^1\Pi_1$–$^3\Sigma_1^+$ potential curve crossing, as expected. There was some $^1\Pi_1$–$^3\Pi_1$ direct coupling at small R, but it was negligible compared with the $^1\Pi_1$–$^3\Sigma_1^+$ coupling. At larger R, where the energy difference between the $^3\Sigma_1^+$ and $^3\Pi_1$ state in the exit channel is smallest, $^3\Sigma_1^+$–$^3\Pi_1$ 'radial' coupling maximized, resulting in a 10% net yield of Zn(4s4p $^3P_1$). The calculations reproduced well the experimentally observed cross-sections (Umemoto *et al.* 1992) for the production of Zn(4s4p $^3P_2$) (3·9 Å^2 as against 3·4 Å^2 observed), Zn(4s4p $^3P_1$) (0·4 Å^2 as against 0·4 Å^2 observed) and Zn(4s4p $^3P_0$) (<0·01 Å^2 as against 0·0 Å^2 observed). These calculations assumed that the spin–orbit coupling constant was that of the Zn(4s4p) states, 386 cm^{-1}, and did *not* vary with R_{ZnXe}; so *no* increase in the effective spin–orbit constant due to the 'heavy-atom' Xe is necessary to account for the results in the Zn·Xe case. Since the spin–orbit constant of the Cd(5s5p) states is even larger, it is obvious that, in the two cases where efficient singlet-to-triplet deactivation by Xe has been observed, namely Zn(4s4p $^1P_1$) and Cd(5s5p $^1P_1$), the spin–orbit coupling due to the metal atoms is quite sufficient to account for the singlet–triplet coupling. Thus Xe serves as a 'large' atom in these processes and *not* a 'heavy' atom.

However, when the spin–orbit coupling constant is *very* low, say 40·6 cm^{-1} for the Mg(3s3p) states, an increase in effective spin–orbit coupling for the $^1\Pi_1$–$^3\Sigma_1^+$ interaction is expected, based on recent spectroscopic results (Breckenridge *et al* 1993). For example, high-resolution LIF studies (Baumann *et al.* 1992) of the analogous Na(3p ^2P_J)·Xe($^2\Sigma_{1/2,3/2}^+$) states show *clearly* that the effective spin–orbit coupling constant is greatly increased compared with the Na(3p ^{2}P) atomic spin–orbit constant of only 11·5 cm^{-1}, the extrapolated value at the bottom of the Na·Xe($^2\Pi_{1/2,3/2}$) potential curves being about 110 cm^{-1}. A similar increase might be expected for the Mg(3s3p $^1P_1$)·Xe($^1\Pi$) state, which could increase the effective $^1\Pi_1$–$^3\Sigma_1^+$ coupling on the order of three times or so. Since *no* Mg(3s3p $^1P_1$)·Xe($^1\Pi_1$) predissociation to Mg(3s3p $^3P_2$) is observed experimentally, then this can only be because the $^1\Pi_1$ and $^3\Sigma_1^+$ curves *do not cross* below the $^1\Pi_1$ dissociation limit, the same conclusion that was reached on the basis of the MgXe($^3\Sigma^+$) potential curve *ab-initio* calculations (Bililign *et al.* 1993).

Acknowledgments

This article is dedicated to my graduate and postdoctoral advisors (in those ancient days) who first sparked my interest in this area of research: Don Baulch, Fred Dainton, Henry Taube and Tony Callear.

Support for the research in the Breckenridge laboratories by the National Science Foundation and the Petroleum Research Fund is gratefully acknowledged.

References

ALEXANDER, M. H., and POUILLY, B., 1988, *Selectivity in Chemical Reactions*, edited by J. C. Whitehead (Dordrecht: Kluwer), p. 265.

BAUMANN, P., ZIMMERMAN, D., and BRÜHL, R., 1992, *J. molec. Spectrosc.*, **155**, 277.

BENNETT, R. R., and BRECKENRIDGE, W. H., 1990, *J. chem. Phys.*, **92**, 1588; 1992, *Ibid.*, **96**, 882.

BENNETT, R. R., MCCAFFREY, J. G., and BRECKENRIDGE, W. H., 1990, *J. chem. Phys.*, **92**, 2740.

BILILIGN, S., GUTOWSKI, M., SIMONS, J., and BRECKENRIDGE, W. H., 1993, *J. chem. Phys.*, **99**, 3815.

BRECKENRIDGE, W. H., 1983, *Reactions of Small Transient Species*, edited by M. Clyne and A. Fontijn (New York: Academic Press); 1989, *Accts. Chem. Res.*, **22**, 21.

BRECKENRIDGE, W. H., JOUVET, C., and SOEP, B., 1986, *J. chem. Phys.*, **84,** 1443; 1994, *Advances in Metal and Semiconductor Clusters*, Vol. III, edited by M. Duncan (Greenwich, CT: JIA Press) (to be published).

BRECKENRIDGE, W. H., and MALMIN, O. K., 1979, *Chem. Phys. Lett.*, **68,** 341; 1981, *J. chem. Phys.*, **74,** 3307.

BRECKENRIDGE, W. H., and MERROW, C. N., 1988, *J. chem. Phys.*, **88,** 2320, 2329.

BRECKENRIDGE, W. H., and UMEMOTO, H., 1982, *The Dynamics of the Excited State*, Advances in Chemical Physics, edited by K. Lawley, Vol. 50 (New York:Wiley).

FUNK, D. J., and BRECKENRIDGE, W. H., 1989, *J. chem. Phys.*, **90,** 2927.

FUNK, D. J., KVARAN, A., and BRECKENRIDGE, W. H., 1989, *J. chem. Phys.*, **90,** 2915.

JOUVET, C., and SOEP, B., 1983, *Chem. Phys. Lett.*, **96,** 426.

KOWALSKI, A., CZAJKOWSKI, M., and BRECKENRIDGE, W. H., 1985, *Chem. Phys. Lett.*, **121,** 217.

KVARAN, A., FUNK, D. J., KOWALSKI, A., and BRECKENRIDGE, W. H., 1988, *J. chem. Phys.*, **89,** 6069.

LAIDLER, K. J., 1942, *J. chem. Phys.*, **10,** 34, 43; 1947, *Ibid.*, **15,** 712.

LEFEBVRE-BRION, H., and FIELD, R. W., 1986, *Perturbations in the Spectra of Diatomic Molecules* (Orlando, FL: Academic Press).

MCCAFFREY, J. G., FUNK, D. J., and BRECKENRIDGE, W. H., 1993, *J. chem. Phys.*, **99,** 9472; 1994, *Ibid.*, **100.**

MCGLYNN, S. P., AZUMI, T., and KINOSHITA, M., 1969, *Molecular Spectroscopy of the Triplet State* (Englewood Cliffs, NJ: Prentice-Hall).

POUILLY, B., and ALEXANDER, M. H., 1987, *J. chem. Phys.*, **86,** 4790.

UMEMOTO, H., OHNUMA, T., IKEDA, H., TSUNASHIMA, S., and KUWAHARA, K., 1992, *J. chem. Phys.*, **97,** 3282.

WALLACE, I., 1991, Ph.D. Thesis, University of Utah.

WALLACE, I., BENNETT, R. R., and BRECKENRIDGE, W. H., 1988, *Chem. Phys. Lett.*, **153,** 127.

WALLACE, I., KAUP, J., and BRECKENRIDGE, W. H., 1991, *J. phys. Chem.*, **95,** 8060.

WALLACE, I., RYTER, J., and BRECKENRIDGE, W. H., 1992, *J. chem. Phys.*, **96,** 136.